RESEARCH ARTICLE

SiO$_x$N$_y$ back-contact barriers for CZTSe thin-film solar cells

Wenjian Chen *, **Hippolyte Hirwa, Jörg Ohland, Teoman Taskesen, Ulf Mikolajczak, Devendra Pareek, Jürgen Parisi, Levent Gütay**

Laboratory for Chalcogenide Photovoltaics, Energy and Semiconductor Research Laboratory, Institute of Physics, Carl von Ossietzky University of Oldenburg, Oldenburg, Lower Saxony, Germany

* wenjian.chen@uni-oldenburg.de

Abstract

The formation of molybdenum diselenide (MoSe$_2$) is widely observed at the back-contact interface for copper zinc tin selenide (CZTSe) thin-film solar cells. Depending on individual selenium (Se) supply and thermal conditions for forming CZTSe absorbers on molybdenum (Mo) substrates, the thickness of MoSe$_2$ can vary from a few hundreds of nanometers up to $\approx$ 1 μm, which is comparable to the commonly adopted thickness of 1 ~ 1.5 μm for CZTSe absorbers. In this study, for controlling the thickness of interfacial MoSe$_2$, thin diffusion barrier layers of silicon oxynitride (SiO$_x$N$_y$) are deposited onto Mo layers prior to the growth of CZTSe absorbers in the fabrication process. As a result, a reduction in the thicknesses of MoSe$_2$ layers is achieved. In terms of energy conversion efficiency (η), CZTSe solar cells grown on Mo/SiO$_x$N$_y$ back contacts suffer a deterioration as the SiO$_x$N$_y$ layers get thicker. CZTSe solar cells grown on Mo/SiO$_x$N$_y$/Mo back contacts preserve their efficiencies at $\approx$ 11% with thin 10 nm SiO$_x$N$_y$ layers.

Introduction

Kesterite Cu$_2$ZnSn(S,Se)$_4$ (CZTSSe) is considered as a promising substitution for chalcopyrite Cu(In,Ga)(Se,S)$_2$ (CIGSSe) in thin-film solar cell technology due to its earth abundant and low-cost constituents [1, 2]. However, in terms of the energy conversion efficiency (η), CZTSSe solar cells reach only 12.6% while CIGSSe devices have an up-to-date record of $\approx$ 23.4% [3, 4]. For pure Cu$_2$ZnSnS$_4$ and Cu$_2$ZnSnSe$_4$ solar cells, the record efficiencies are reported to be 11% and 12.5%, respectively [5, 6]. In order to further improve kesterite solar cells, addressing the back-contact issues is important, especially for pure CZTSe devices. By replacing CIGSSe with CZTSSe as the absorber material, molybdenum (Mo) is generally inherited as the back-contact material [7]. In most of the reported CZTSe synthesis processes, a MoSe$_2$ layer with a thickness ranging from a few hundred nm up to $\approx$ 1 μm is observed at the Mo/CZTSe back-contact interface [8–10]. In general, the formation of such thick MoSe$_2$ layers is considered to cause negative impacts on the device performance [10, 11]. And for the reported record 12.5% CZTSe solar cell, the MoSe$_2$ thickness is at around 100 ~ 200 nm [6]. Therefore, the limiting and/or control of MoSe$_2$ thickness at the back

interface is commonly discussed as a possible way to improve the solar cell efficiency. Diffusion barriers are commonly adopted with back-contact structure Mo/barrier or Mo/barrier/Mo to avoid or suppress the formation of MoSe$_2$ layers in kesterite solar cells [10, 12, 13]. As for silicon (Si) based microelectronic devices, silicon oxynitride (SiO$_x$N$_y$) is a widely used passivation material. With properties such as high temperature durability, high oxidation resistance and low defect density, it has the benefit of good availability in many research institutions [14, 15]. In this study, we deposit SiO$_x$N$_y$ layers as diffusion barriers with Mo/SiO$_x$N$_y$ and Mo/SiO$_x$N$_y$/Mo back-contact structures. For the as-grown CZTSe solar cells, we show and discuss the results in terms of back-interface morphology, solar cell performance and defect properties.

Materials and methods

Sample preparation

Two types of back-contact structures with SiO$_x$N$_y$ layers were applied: Mo/SiO$_x$N$_y$ and Mo/SiO$_x$N$_y$/Mo. As shown in Fig 1, a standard Mo layer ($\approx$ 550 nm) consisting of two sub-layers ($\approx$ 275 nm for each) was deposited by Ar plasma (power density: 6.1 W/cm^2, pressure: 2.7×10^{-3} mbar) onto the 1 mm soda lime glass (SLG). SiO$_x$N$_y$ layers (10, 25 and 40 nm) were deposited from Si sputter target by mixed Ar-N$_2$-O$_2$ plasma (power: 160 W, pressure: 2×10^{-3} mbar) onto the standard Mo layers. For Mo/SiO$_x$N$_y$/Mo back-contact structure, the top Mo layer ($\approx$ 50 nm) on SiO$_x$N$_y$ was deposited under the same conditions as for the standard Mo layers. For both back-contact structures, a standard procedure for the fabrication of solar cells in our lab was performed [8, 16, 17]. In this study, a dry cleaning with Ar plasma (power: 100 W, pressure: 5×10^{-3} mbar, duration: 90 s) was performed on the as-grown Mo/SiO$_x$N$_y$ and Mo/SiO$_x$N$_y$/Mo back contacts. For the formation of CZTSe absorber, a metallic precursor with a structure of Zn/Cu-Sn/Zn was deposited onto the above-mentioned back contacts by DC-sputtering at room temperature, followed by the annealing with selenium (Se) pellets and tin (Sn) wires in a tube
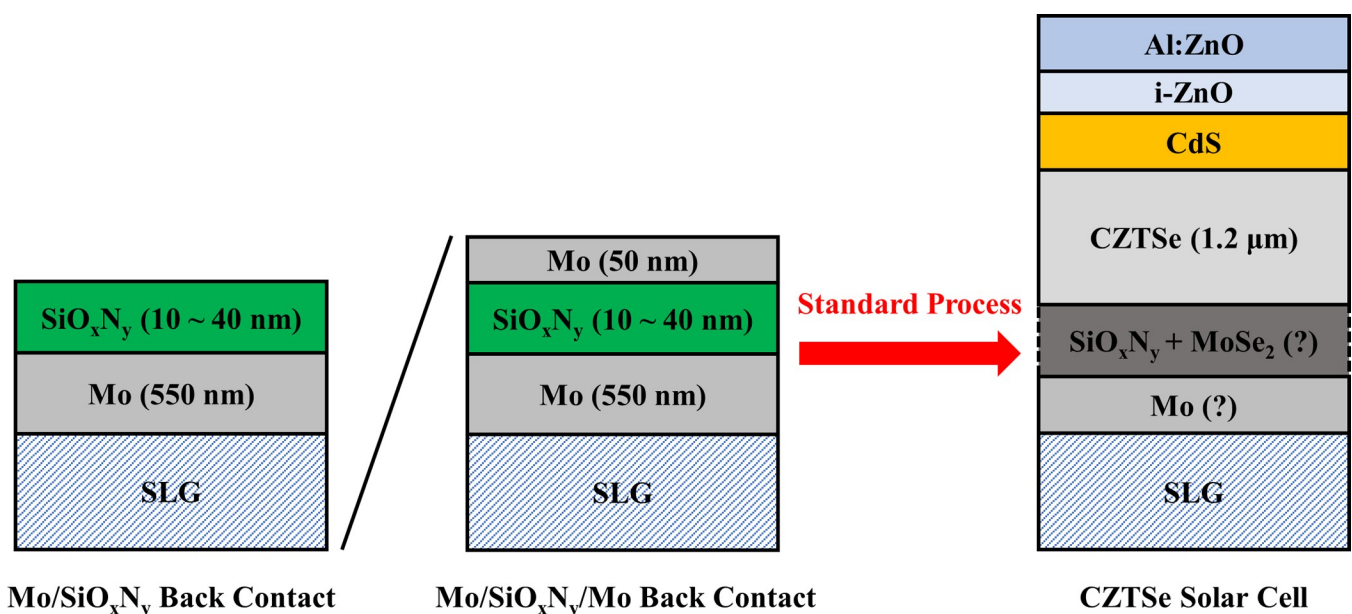
Fig 1. Schematic diagram of CZTSe solar cells grown with SiO$_x$N$_y$ back-contact barriers.

furnace at 530˚C for 20 minutes. As buffer layers, cadmium sulfide (CdS) was deposited onto the as-grown CZTSe absorbers (≈ 1.2 µm) via chemical bath. Furthermore, i-ZnO and Al:ZnO layers were deposited by RF-sputtering as front contacts. Finally, every sample was divided by mechanical scribing into solar cells with an average area of ≈ 0.25 cm^2. In the following statement, the reference solar cell with a standard 550 nm Mo back contact is denoted by "M". The solar cells grown on Mo/SiO_xN_y back contacts are denoted by "MS10", "MS25" and "MS40", for which the thicknesses of SiO_xN_y layers are 10, 25 and 40 nm, respectively. "MM" denotes the reference solar cell with a Mo/Mo back contact, in which a top layer of Mo (≈ 50 nm) is deposited on the standard Mo layer. "MS10M", "MS25M" and "MS40M" denote solar cells grown on Mo/SiO_xN_y/Mo back contacts, in which the thicknesses of SiO_xN_y layers between the top and the standard Mo layers are 10, 25 and 40 nm, respectively.
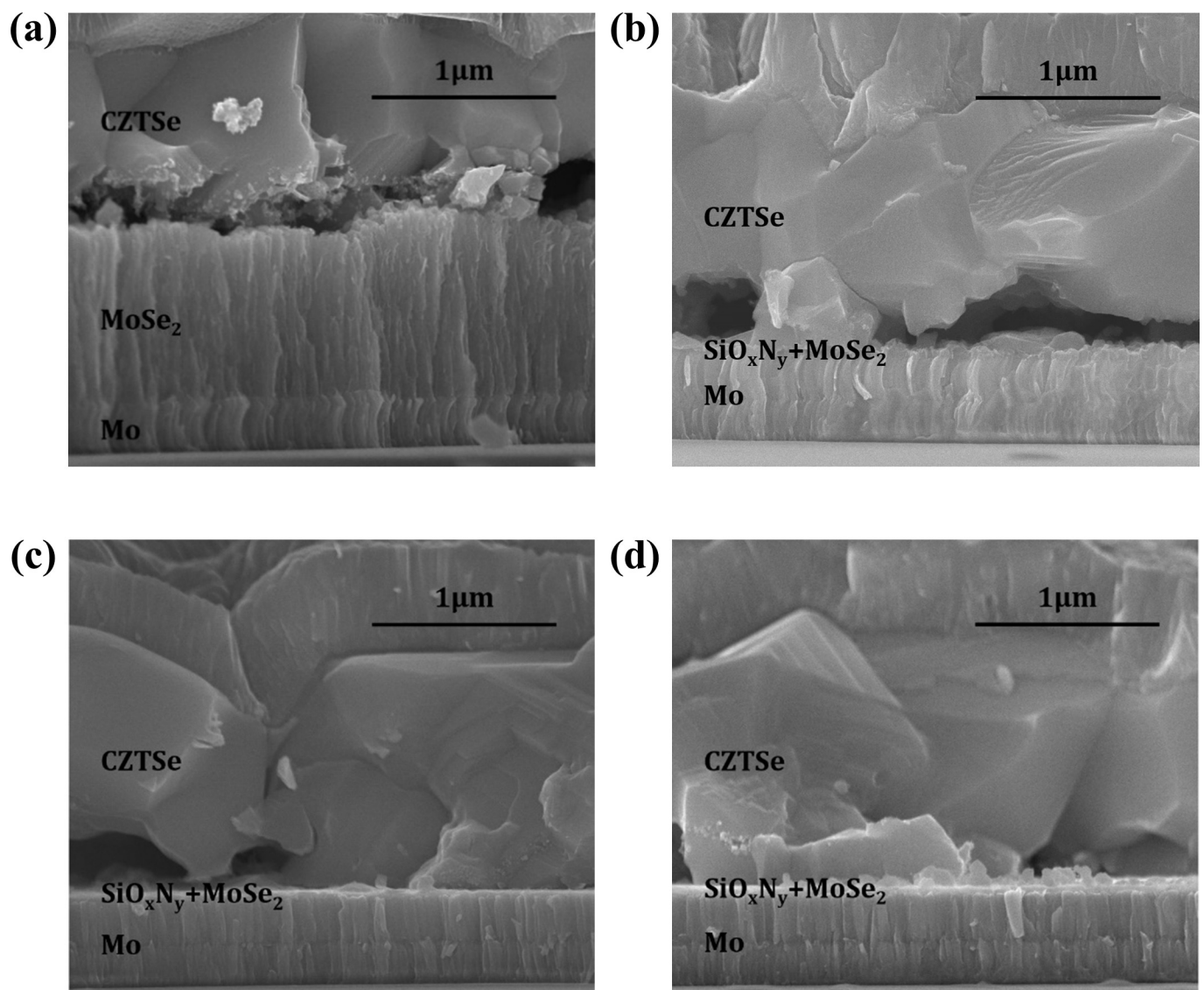
Fig 2. SEM cross-section of CZTSe solar cells grown on Mo and Mo/SiO_xN_y back contacts. Images are captured for samples **(a)** M, **(b)** MS10, **(c)** MS25 and **(d)** MS40, respectively.

https://doi.org/10.1371/journal.pone.0245390.g002

Characterization

A FEI Helios Nanolab 600i scanning electron microscope (SEM) was used for the characterization of cross-section morphology. A Keithley 2400 SMU was adopted for current-voltage (*I-V*) measurements of CZTSe solar cells under standard AM 1.5 illumination in a PET SS100AAA solar simulator. A Bentham PVE300 system was used for EQE measurements. Measurements of capacitance-frequency (*C-f*) and thermal admittance spectroscopy (TAS) were performed with a Solartron impedance analyzer SI-1260. The admittance spectra were recorded for a frequency range from 10 Hz to 1 MHz and a temperature range from 50 K to 330 K. The processes of heating and cooling were performed in a closed cycle Helium cryostat at a base pressure $< 10^{-5}$ mbar. For precise measurements of the temperature, a thermal sensor was glued on top of a dummy cell placed next to the real sample.

Results and discussion

Mo/SiO_xN_y back contact

Fig 2 shows SEM cross-section morphology of CZTSe samples grown on Mo and Mo/SiO_xN_y back contacts. The reference sample M, which has no SiO_xN_y diffusion-barrier layer, shows the formation of a $\approx$ 1 μm $MoSe_2$ interfacial layer. Samples with SiO_xN_y layers in various
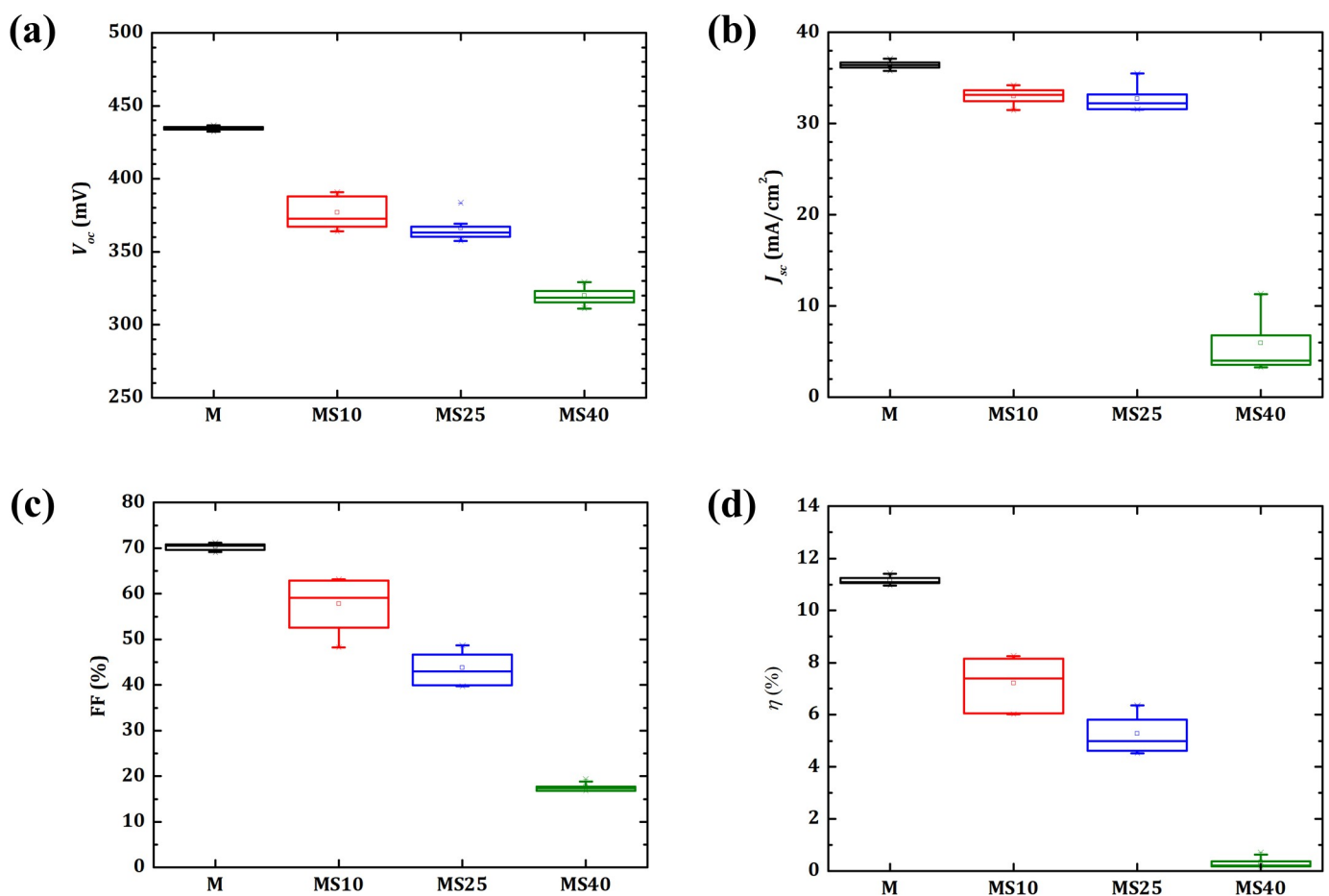
Fig 3. Parameters of CZTSe solar cells grown on Mo and Mo/SiO_xN_y back contacts. Boxplots of solar cell parameters **(a)** V_{oc}, **(b)** J_{sc}, **(c)** FF and **(d)** η for every type of back contacts include data from 6 to 9 cells.

thicknesses (i.e., 10, 25 and 40 nm) show a significantly suppressed formation of $MoSe_2$ layers. The specific thicknesses of formed $MoSe_2$ layers lie in the range of 30 ~ 40 nm with no visible trend. This suggests that SiO_xN_y acts as an effective diffusion barrier for Se and prevents the strong reaction of Mo and Se to form $MoSe_2$ during a high temperature ($\approx$ 530°C) annealing.

Performance of the CZTSe solar cells grown on Mo and Mo/SiO_xN_y back contacts are shown in Fig 3. Compared to the reference M, which is grown on pure Mo back contact, all the solar cells from Mo/SiO_xN_y back contacts show a deterioration in all parameters, i.e., open-circuit voltage (V_{oc}), short-circuit current density (J_{sc}), fill factor (FF) and energy conversion efficiency (η). The reasons for the observed deterioration of solar cell properties may include a possible formation of an extra potential barrier induced by SiO_xN_y layers. Furthermore, it cannot be excluded that a small amount of oxygen atoms from SiO_xN_y may diffuse into the CZTSe absorbers and lead to additional impurity states in the absorber, which could impact the defect landscape or influence the phase structure of kesterite material in relevant regions. Moreover, thicker SiO_xN_y diffusion barriers may further cause a harmful influence on the device performance by blocking sodium diffusion from SLG, which is generally considered to enhance the absorber quality in CIGS and kesterite solar cells [18–20]. However, based on our previous research, in which SiO_xN_y was investigated as barrier layers between SLG and Mo, a total blocking effect for sodium was only achieved with much thicker SiO_xN_y layers [21]. That means the blocking effect of SiO_xN_y layers for sodium have most probably only a very minor influence in the present case. As a consequence, the CZTSe solar cells grown on Mo/
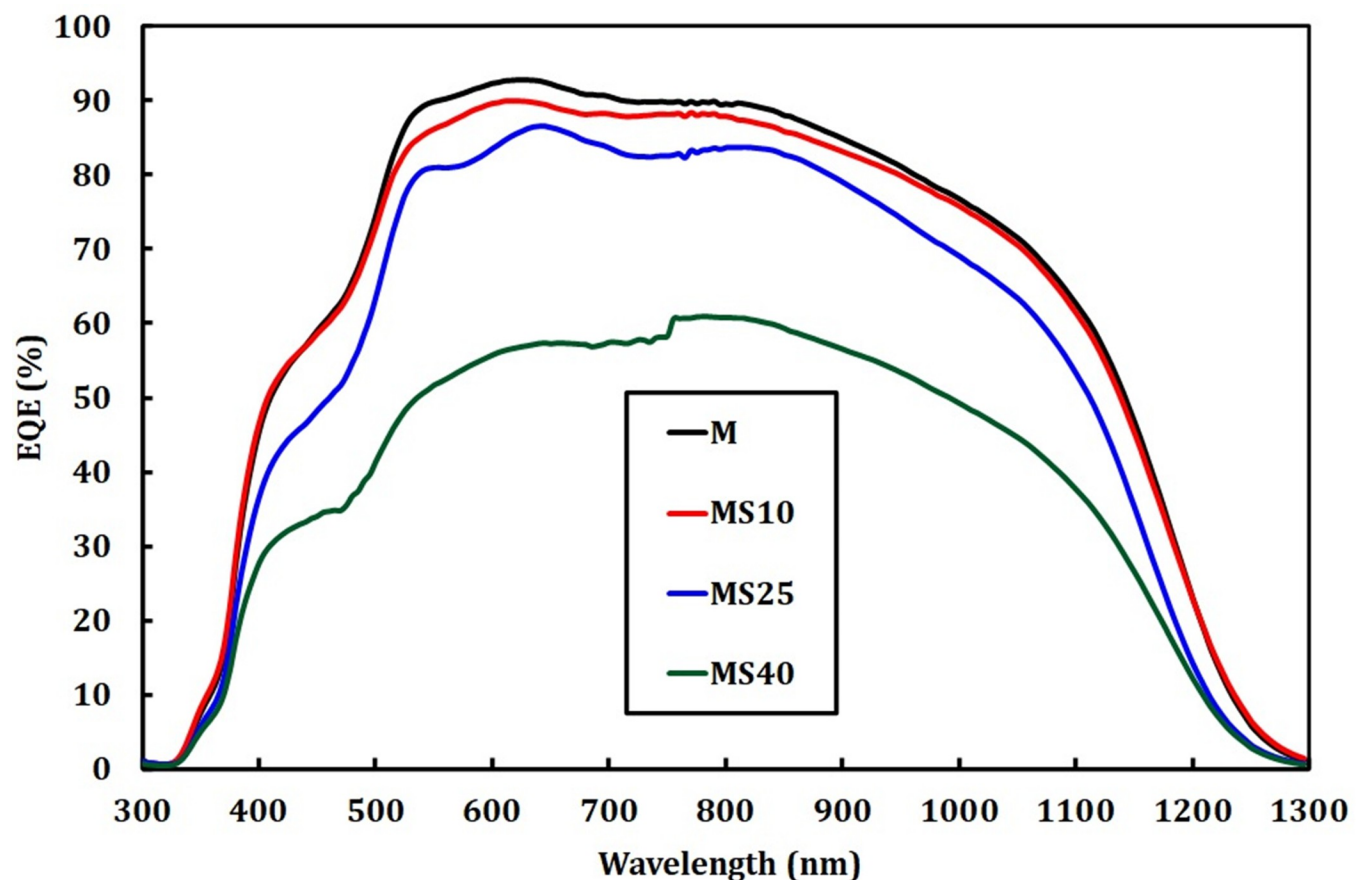
Fig 4. EQE measurements of CZTSe solar cells grown on Mo and Mo/SiO_xN_y back contacts.
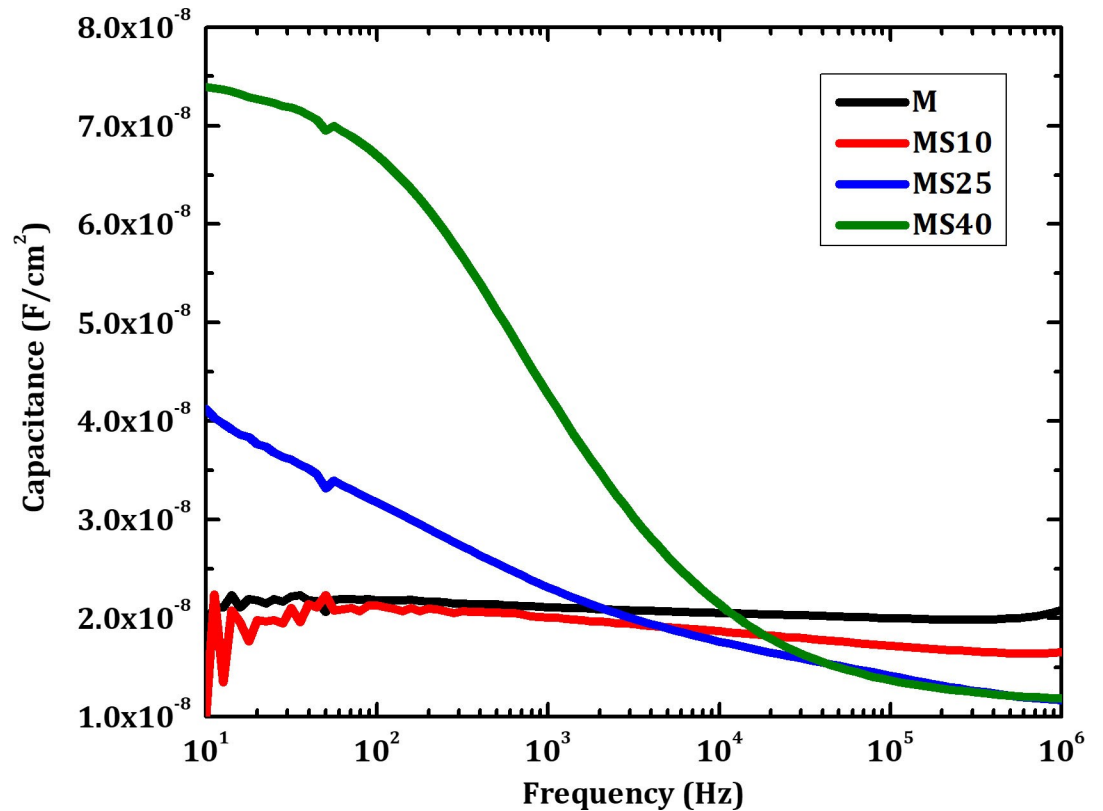
Fig 5. C-f measurements of CZTSe solar cells grown on Mo and Mo/SiO$_x$N$_y$ back contacts.

SiO$_x$N$_y$ back contacts show overall poor performance, regardless of a possible positive effect expected from the reduced thicknesses of MoSe$_2$ layers.
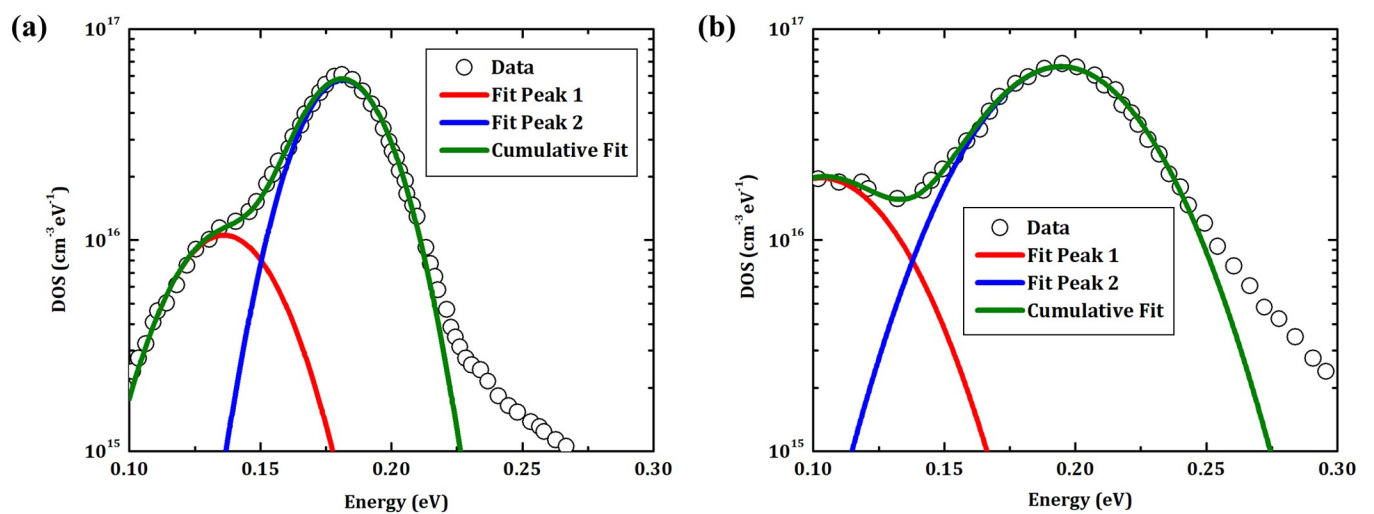
Fig 6. Density of states for CZTSe solar cells grown on Mo and Mo/SiO$_x$N$_y$ back contacts. DOS are derived from TAS measurements on samples **(a)** M and **(b)** MS40, respectively.

Fig 4 shows the EQE of CZTSe solar cells grown on Mo and Mo/SiO_xN_y back contacts. The overall EQE drops for the samples with SiO_xN_y layers compared to that of the reference. Specifically, MS10 and MS25 show a slight drop while MS40 shows a strong one. This result matches the performance shown in the previous *I-V* measurements. In particular for the sample MS40, the strong drop in EQE and in the extracted short-circuit current (S1 Fig) suggest not only an increased series resistance, for which the EQE drop is wavelength independent, but also a potential barrier introduced by the thick SiO_xN_y layer and/or a deterioration in absorber quality.

Fig 5 shows results from *C-f* measurements of CZTSe solar cells grown on Mo and Mo/SiO_xN_y back contacts. According to literature about similar material-systems, inflection points related to shallow defects can be observed in capacitance measurements between 10 Hz and 100 kHz at temperatures between 50 K and 200 K [22–25]. In our case, samples M and MS10
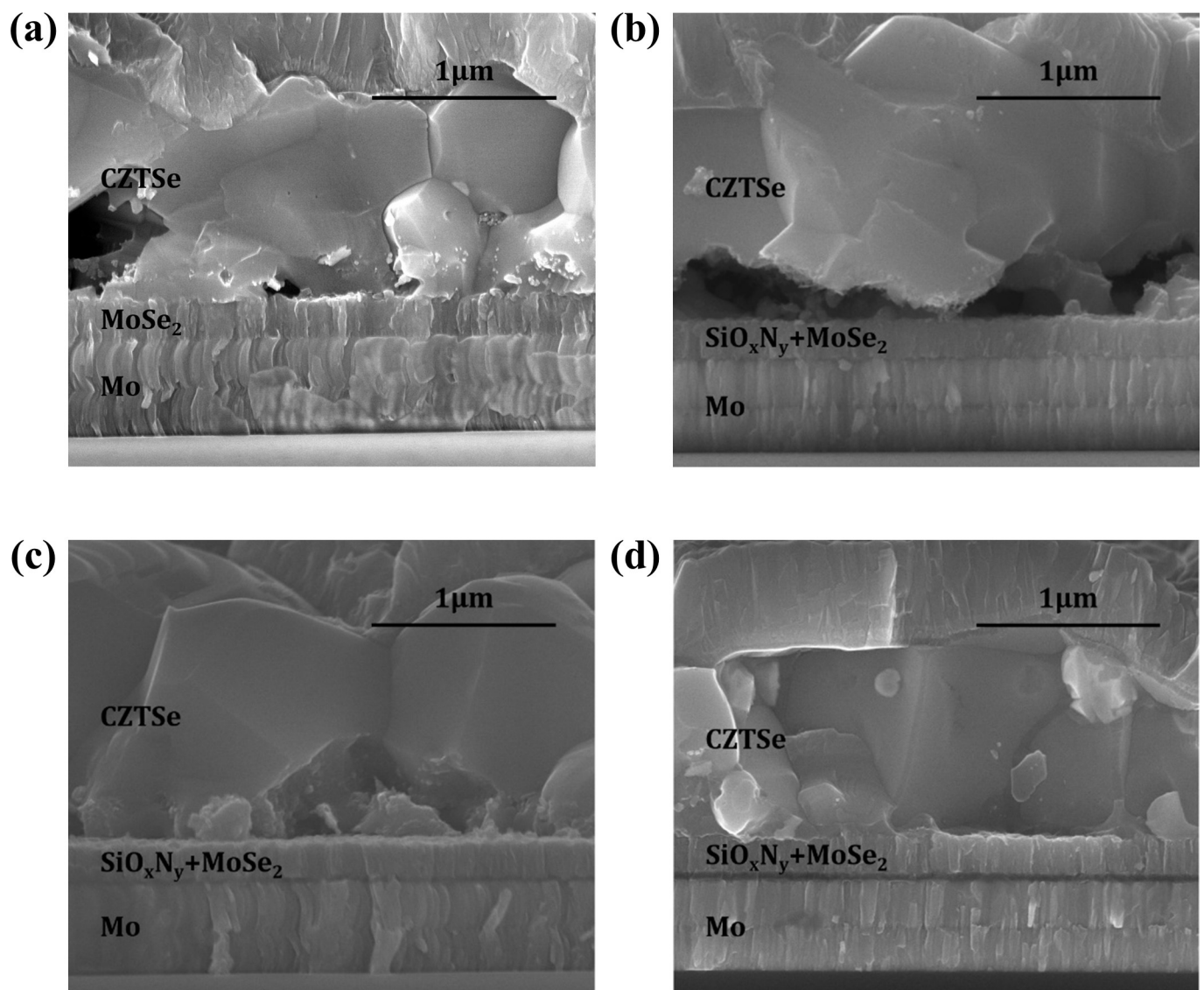
Fig 7. SEM cross-section of CZTSe solar cells grown on Mo/Mo and Mo/SiO_xN_y/Mo back contacts. Images are captured for samples **(a)** MM, **(b)** MS10M, **(c)** MS25M and **(d)** MS40M, respectively.

https://doi.org/10.1371/journal.pone.0245390.g007

do not show clear inflection points. Samples MS25 and MS40, which are grown on back contacts with thicker SiO$_x$N$_y$ layers, show clear inflection points. This may suggest a higher defect-density for CZTSe solar cells grown on Mo/SiO$_x$N$_y$ back contacts with the thicker SiO$_x$N$_y$ layers. Specific distributions of defects are investigated by TAS measurements and shown in the following part.

Density of states (DOS) derived from TAS measurements on CZTSe solar cells M and MS40 are shown in Fig 6. The results of sample M, as shown in Fig 6A, reveal a small peak at ≈ 0.13 eV and a large peak at ≈ 0.18 eV. For sample MS40, as shown in Fig 6B, both peaks are broadened in comparison to the previous case and their maxima are shifted to ≈ 0.10 eV and ≈ 0.20 eV, respectively. According to literature based on Cu$_2$ZnSn(S,Se)$_4$, both peaks may be linked to bulk defects [22, 25]. The significant broadening of the deeper defect is visibly accompanied by an enhanced density of states at deeper levels, which could cause higher recombination rates and thus a deterioration of solar cell properties.

Mo/SiO$_x$N$_y$/Mo back contact

Cross-section morphology of CZTSe solar cells grown on Mo/Mo and Mo/SiO$_x$N$_y$/Mo back contacts is shown Fig 7. In comparison to the case of sample M, the thicknesses of interfacial
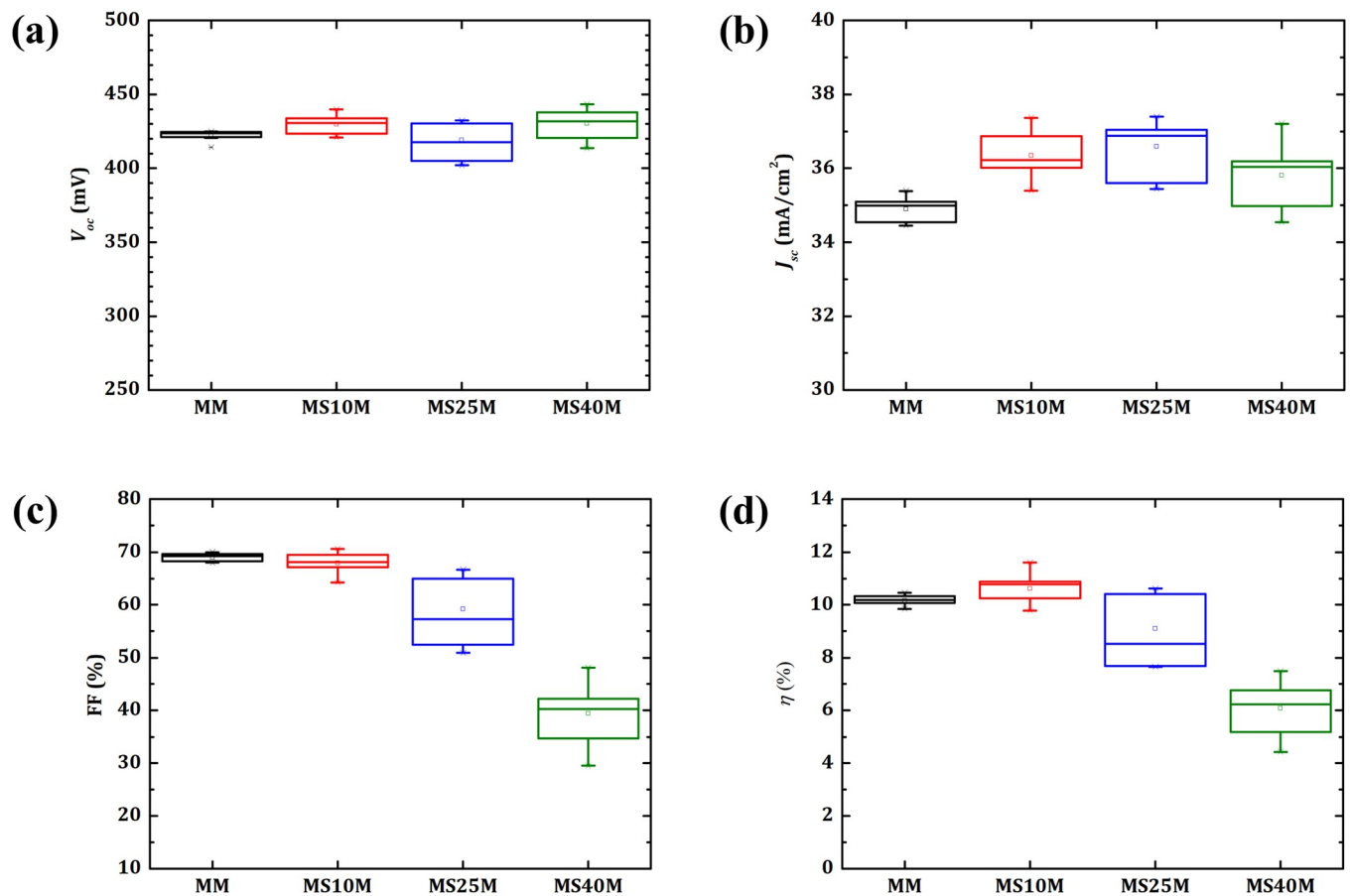
Fig 8. Parameters of CZTSe solar cells grown on Mo/Mo and Mo/SiO$_x$N$_y$/Mo back contacts. Boxplots of solar cell parameters **(a)** V_{oc}, **(b)** J_{sc}, **(c)** FF and **(d)** η for every type of back contacts include data from 6 to 9 cells.

MoSe$_2$ layers of MS10M, MS25M and MS40M are reduced to a range of 230 ~ 240 nm with no obvious trend for the thicknesses of the investigated SiO$_x$N$_y$ layers. It indicates that only the top Mo layers ($\approx$ 50 nm) in Mo/SiO$_x$N$_y$/Mo structures contribute to the formation of MoSe$_2$ layers during the annealing and the Mo layers ($\approx$ 550 nm) underneath SiO$_x$N$_y$ barriers remain intact. Surprisingly, for the reference sample MM, in which no barrier is applied, the thickness of interfacial MoSe$_2$ stays also in a similar range as for the samples grown on Mo/SiO$_x$N$_y$/Mo back contacts. This indicates a barrier-like behavior at the Mo/Mo interface, which could be related to a natural passivation due to the process-break in Mo fabrication or a blocking effect due to crystal discontinuity in this layered structure.

Fig 8 shows parameters of CZTSe solar cells grown on Mo/Mo and Mo/SiO$_x$N$_y$/Mo back contacts. For the sample MS10M, all the device parameters (V_{oc}, J_{sc}, FF and η) stay in a similar or slightly improved range in comparison to the reference MM. In cases of thicker SiO$_x$N$_y$ layers (MS25M and MS40M), the device performance deteriorates. However, the deterioration here may differ from the samples grown on Mo/SiO$_x$N$_y$ back contacts. In cases of Mo/SiO$_x$N$_y$ back contacts, the deterioration could possibly be a combined result from the negative influence of SiO$_x$N$_y$ at the back interface and the deteriorated CZTSe absorber quality. For Mo/SiO$_x$N$_y$/Mo back contacts, a thin SiO$_x$N$_y$ layer may have a positive effect due to its role as passivation layer in between the formed porous MoSe$_2$ and the intact
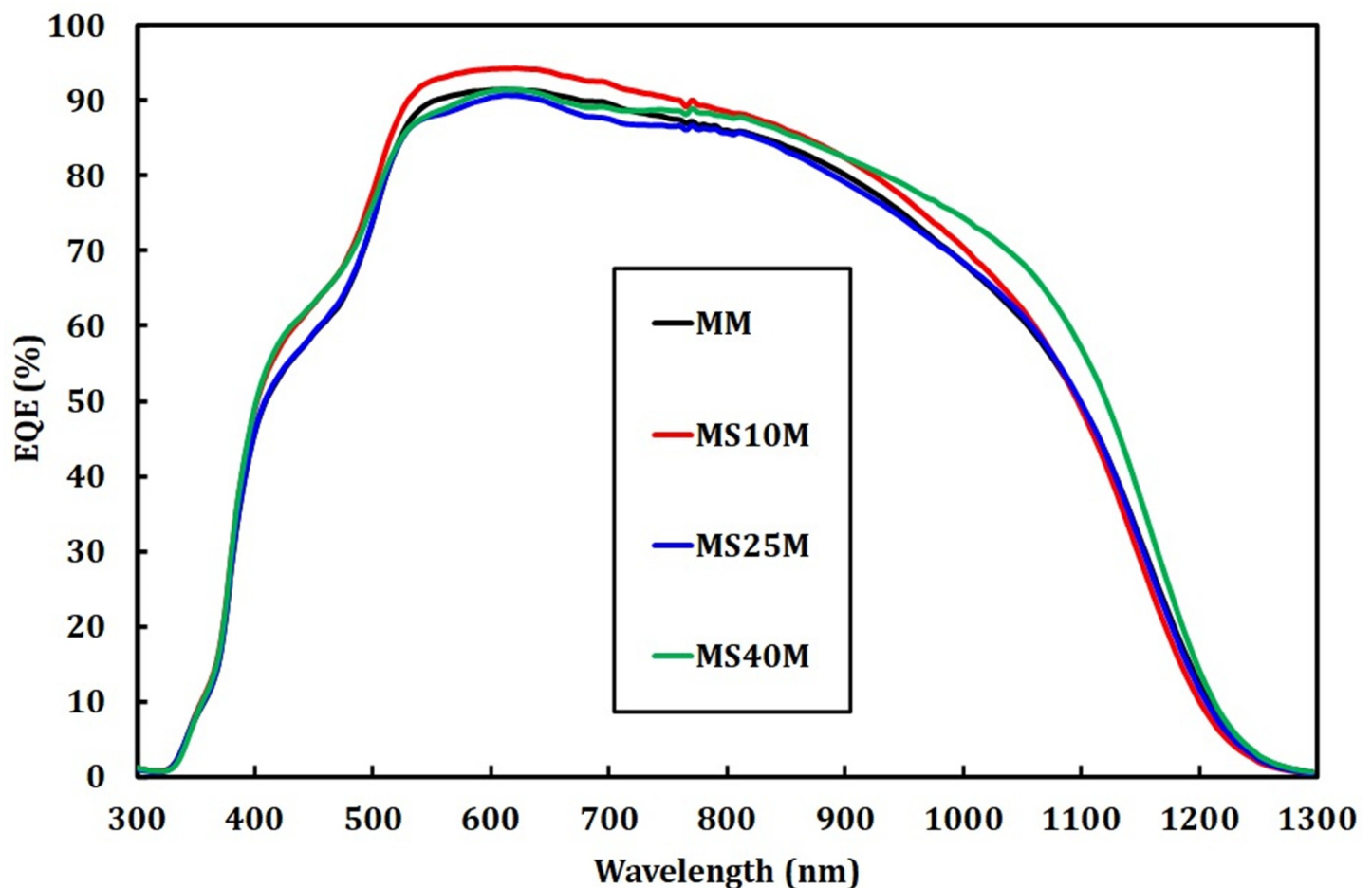
Fig 9. EQE measurements of CZTSe solar cells grown on Mo/Mo and Mo/SiO$_x$N$_y$/Mo back contacts.

bottom Mo, which could compensate the disadvantages such as causing an electrical barrier or an extra series resistance. As a result, for MS10M, without a noticeable drawback in FF, a similar V_{oc} and a small increase in J_{sc} lead to an improved η at around 11% in comparison to the case of MM. And compared to M, MS10M gives a similar η with a higher homogeneity in the morphology at the back interface. However, for the cases of MS25M and MS40M, in which the SiO$_x$N$_y$ layers are thicker, the possible negative effects of SiO$_x$N$_y$ on the back interface and the CZTSe absorber quality dominate and cause a significant drop in FF thus the η of the whole devices.

Fig 9 shows EQE of CZTSe solar cells grown on Mo/Mo and Mo/SiO$_x$N$_y$/Mo back contacts. Compared to that of the previous samples grown on Mo/SiO$_x$N$_y$ back contacts, the change in thicknesses of the added SiO$_x$N$_y$ layers has a much smaller impact on the EQE, which shows no clear trend. This indicates that the negative effects of a thick SiO$_x$N$_y$ layer are significantly reduced by applying a 50 nm Mo layer on top. EQE of all devices reach $\approx$ 90% at around 600 nm. The extracted values of J_{sc} remain constant at around 35 mA/cm^2 (S2 Fig).

Fig 10 shows C-f measurements of CZTSe solar cells grown on Mo/Mo and Mo/SiO$_x$N$_y$/Mo back contacts. Compared to that of the samples without the 50 nm Mo top layers, no clear inflection point is observed for all the samples grown on Mo/SiO$_x$N$_y$/Mo back contacts. This result is consistent with the above-discussed I-V and EQE measurements, suggesting that the additional Mo layers on top of the SiO$_x$N$_y$ can suppress or compensate the negative impacts from SiO$_x$N$_y$ layers. The presence of MoSe$_2$ may have beneficial effects on the overall interface
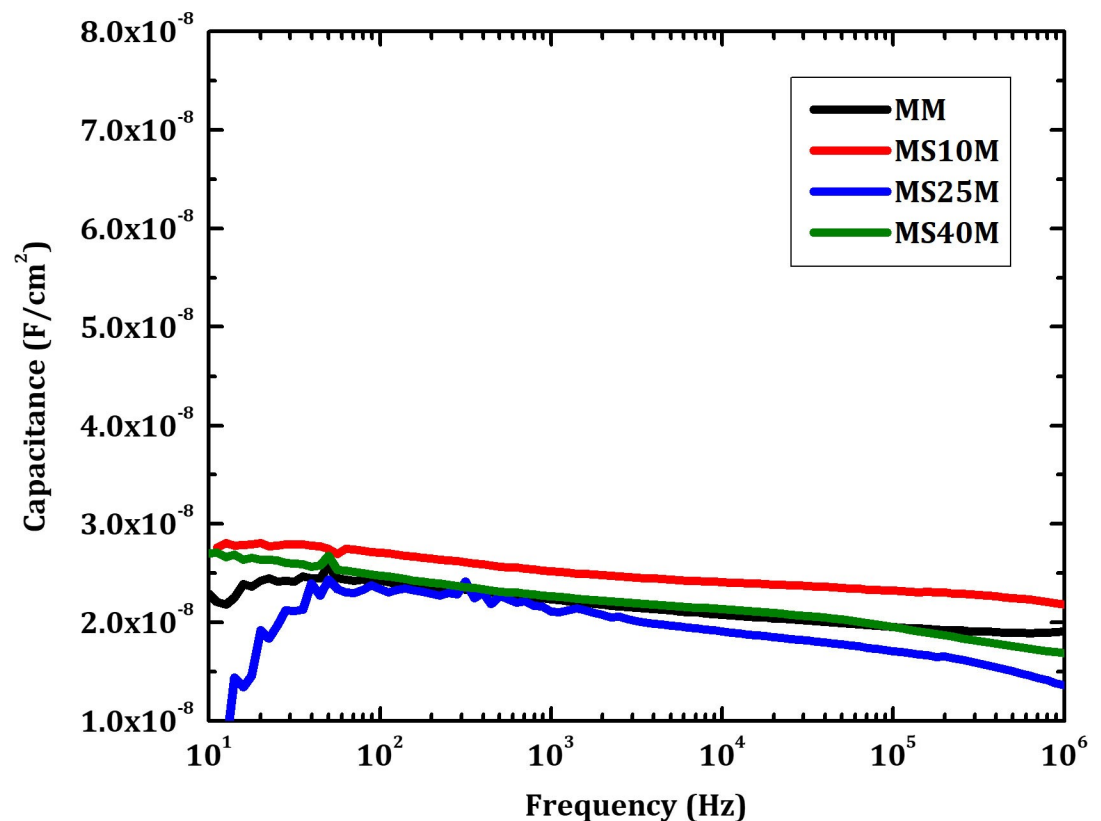
Fig 10. C-f measurements of CZTSe solar cells grown on Mo/Mo and Mo/SiO$_x$N$_y$/Mo back contacts.
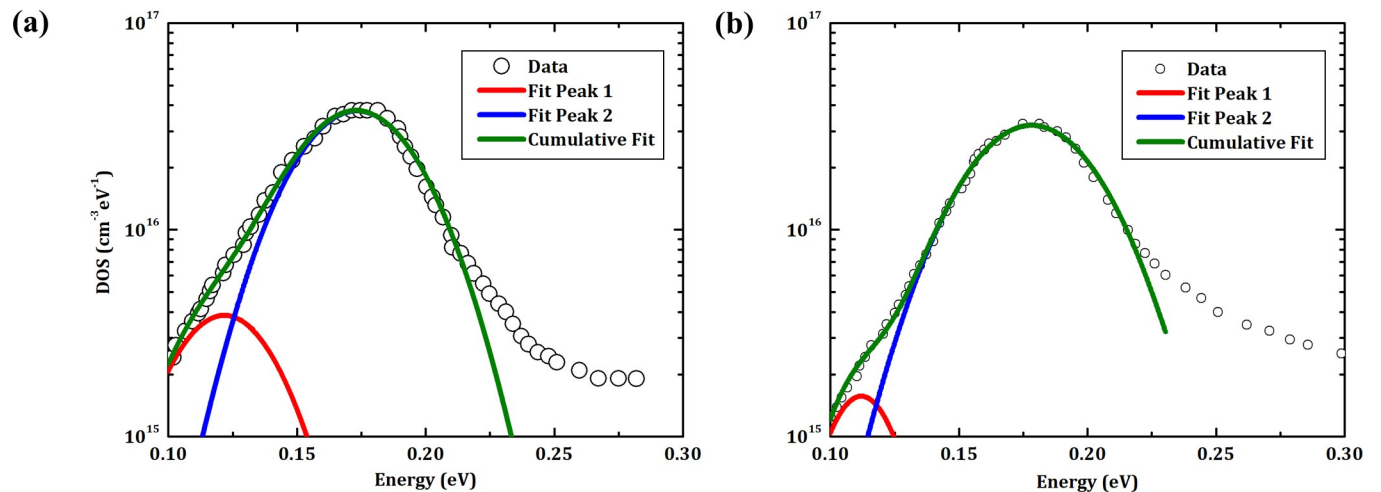
Fig 11. Density of states for CZTSe solar cells grown on Mo/Mo and Mo/SiO$_x$N$_y$/Mo back contacts. DOS are derived from TAS measurements on samples (**a**) MM and (**b**) MS40M, respectively.

https://doi.org/10.1371/journal.pone.0245390.g011

quality due to a more favorable alignment of the work functions and hence the bands of the adjacent layers.

Fig 11 shows the DOS derived from TAS measurements of the CZTSe solar cells MM and MS40M. In comparison with Fig 6, the overall influence of SiO$_x$N$_y$ on DOS is much smaller. In details, compared to the case of MM, the small peak at ≈ 0.12 eV is reduced and the large peak at ≈ 0.18 eV is slightly broader for MS40M. If the shallow levels at ≈ 0.12 eV is related to the interface defects, this result could indicate that SiO$_x$N$_y$ is beneficial for suppressing interface defects. However, the slight broadening of the deep levels at ≈ 0.18 eV still may indicate a negative influence of SiO$_x$N$_y$ on raising CZTSe bulk defects. As a result, the combined outcome from the changes at back interface and in absorber bulk is reflected in the device performance.

Conclusions

Our study shows that SiO$_x$N$_y$ can act as an effective diffusion barrier for Se, thus significantly suppressing the formation of MoSe$_2$ at Mo/CZTSe back-contact interface. For CZTSe solar cells grown on Mo/SiO$_x$N$_y$ back contacts, device parameters deteriorate with the increasing thicknesses of SiO$_x$N$_y$ layers. The incorporation of a SiO$_x$N$_y$ barrier layer could not only influence the Mo/CZTSe back-contact interface but also the CZTSe absorber. In cases of Mo/SiO$_x$N$_y$/Mo back contacts, the performance of CZTSe solar cells remain unchanged or slightly improved in the range of $\approx 11\%$ for the adoption of 10 nm SiO$_x$N$_y$ layers. As the SiO$_x$N$_y$ layers gets thicker, the efficiencies of the solar cells decrease much less in comparison to the Mo/SiO$_x$N$_y$ cases. Overall, rather than the MoSe$_2$ thickness, the behavior of back-contact interfaces as well as the absorber quality seem to be the crucial factors influencing the performance of kesterite solar cells.

Supporting information

S1 Fig. J_{sc} extracted from EQE measurements of CZTSe solar cells grown on Mo and Mo/SiO$_x$N$_y$ back contacts.
(TIF)

S2 Fig. *J$_{sc}$* **extracted from EQE measurements of CZTSe solar cells grown on Mo/Mo and Mo/SiO$_x$N$_y$/Mo back contacts.**
(TIF)

Acknowledgments

Author Contributions

Conceptualization: Wenjian Chen, Jörg Ohland, Levent Gütay.

Data curation: Wenjian Chen, Hippolyte Hirwa, Jörg Ohland, Ulf Mikolajczak.

Formal analysis: Hippolyte Hirwa.

Funding acquisition: Wenjian Chen, Teoman Taskesen.

Investigation: Wenjian Chen, Devendra Pareek, Levent Gütay.

Methodology: Wenjian Chen, Hippolyte Hirwa, Jörg Ohland, Teoman Taskesen, Ulf Mikolajczak.

Project administration: Jürgen Parisi, Levent Gütay.

Resources: Jürgen Parisi, Levent Gütay.

Software: Wenjian Chen, Hippolyte Hirwa, Jörg Ohland.

Supervision: Jürgen Parisi, Levent Gütay.

Validation: Teoman Taskesen, Ulf Mikolajczak, Devendra Pareek.

Visualization: Wenjian Chen, Hippolyte Hirwa, Jörg Ohland.

Writing – original draft: Wenjian Chen.

Writing – review & editing: Wenjian Chen, Hippolyte Hirwa, Jörg Ohland, Teoman Taskesen, Ulf Mikolajczak, Devendra Pareek, Jürgen Parisi, Levent Gütay.

References

1. Siebentritt S, Schorr S. Kesterites-a challenging material for solar cells. Prog. Photovolt: Res. Appl. 2012; 20:512–519.

2. Delbos S. Kësterite thin films for photovoltaics: a review. EPJ Photovolt. 2012; 3:35004.

3. Wang W, Winkler MT, Gunawan O, Gokmen T, Todorov TK, Zhu Y, et al. Device characteristics of CZTSSe thin-film solar cells with 12.6% efficiency. Adv. Energy Mater. 2014; 4:1301465.

4. Nakamura M, Yamaguchi K, Kimoto Y, Yasaki Y, Kato T, Sugimoto H. Cd-Free Cu(In,Ga)(Se,S)$_2$ thin-film solar cell with record efficiency of 23.35%. IEEE J. Photovolt. 2019; 9(6):1863–1867.

5. Yan C, Huang J, Sun K, Johnston S, Zhang Y, Sun H, et al. Cu2ZnSnS4 solar cells with over 10% power conversion efficiency enabled by heterojunction heat treatment. Nat. Energy. 2018; 3(9):764–772.

6. Li J, Huang Y, Huang J, Liang G, Zhang Y, Rey G, et al. Defect control for 12.5% efficiency Cu$_2$ZnSnSe$_4$ kesterite thin-film solar cells by engineering of local chemical environment. Adv. Mater. 2020;Nov: e2005268. https://doi.org/10.1002/adma.202005268 PMID: 33185295

7. Gu HJ, Yang J-H, Chen SY, Xiang HJ, Gong XG. Interfacial engineering to improve Cu2ZnSnX4 (X = S, Se) solar cell efficiency. APL Mater. 2019; 7:091104.

8. Taskesen T, Neerken J, Schoneberg J, Pareek D, Steininger V., Parisi J, et al. Device characteristics of an 11.4% CZTSe solar cell fabricated from sputtered precursors. Adv. Energy Mater. 2018; 8:1703295.

9. Brammertz G, Buffière M, Oueslati S, ElAnzeery H, Ben Messaoud K, Sahayaraj S, et al. Characterization of defects in 9.7% efficient Cu$_2$ZnSnSe$_4$-CdS-ZnO solar cells. Appl. Phys. Lett. 2013; 103:163904.

10. Shin B, Zhu Y, Bojarczuk NA, Chey SJ, Guha S. Control of an interfacial MoSe$_2$ layer in Cu$_2$ZnSnSe$_4$ thin film solar cells: 8.9% power conversion efficiency with a TiN diffusion barrier. Appl. Phys. Lett. 2012; 101:053903.

11. Li J, Zhang Y, Zhao W, Nam D, Cheong H, Wu L, et al. A temporary barrier effect of the alloy layer during selenization: tailoring the thickness of MoSe2 for efficient Cu2ZnSnSe4 solar cells. Adv. Energy Mater. 2015; 5:1402178.

12. Schnabel T, Ahlswede E. On the interface between kesterite absorber and Mo back contact and its impact on solution-processed thin-film solar cells. Sol. Energy Mater. Sol. Cells. 2017; 159:290–295.

13. Oueslati S, Brammertz G, Buffière M, ElAnzeery H, Mangin D, ElDaif O, et al. Study of alternative back contacts for thin film Cu$_2$ZnSnSe$_4$-based solar cells. J. Phys. D: Appl. Phys. 2015; 48:035103.

14. Shi Y, He L, Guang F, Li L, Xin Z, Liu R. A review: preparation, performance, and applications of silicon oxynitride film. Micromachines. 2019; 10:552.

15. Balaji N, Lee S, Park C, Raja J, Nguyen HTT, Chatterjee S, et al. Surface passivation of boron emitters on n-type c-Si solar cells using silicon dioxide and a PECVD silicon oxynitride stack. RSC Adv. 2016; 6:70040.

16. Taskesen T, Steininger V, Chen W, Ohland J, Mikolajczak U, Pareek D, et al. Resilient and reproducible processing for CZTSe solar cells in the range of 10%. Prog. Photovolt. Res. Appl. 2018;1–4.

17. Chen W, Taskesen T, Nowak D, Mikolajczak U, Sayed MH, Pareek D, et al. Modifications of the CZTSe/Mo back-contact interface by plasma treatments. RSC Adv. 2019; 9(46):26850–26855.

18. Sadono A, Hino M, Ichikawa M, Yamamoto K, Kurokawa Y, Konagai M, et al. Flexible Cu(In,Ga)Se2 solar cells fabricated using a polyimide-coated soda-lime glass structure. Jpn. J. Appl. Phys. 2015; 54:08KC16.

19. Liu F, Huang J, Sun K, Yan C, Shen Y, Park J, et al. Beyond 8% ultrathin kesterite Cu2ZnSnS4 solar cells by interface reaction route controlling and self-organized nanopattern at the back contact. NPG Asia Mater. 2017; 9(7):e401.

20. Grini S, Sopiha KV, Ross N, Liu X, Bjørheim TS, Platzer-Björkman C, et al. Strong interplay between sodium and oxygen in kesterite absorbers: complex formation, incorporation, and tailoring depth distributions. Adv. Energy Mater. 2019; 9:1900740.

21. Ohland J, Seyfert U. PLASMA-CIGS: Entwicklung eines plasmagestützten Chalkogenisierungsverfahrens zur Herstellung von Cu(In,Ga)(Se,S)-Dünnschichtsolarzellen (PLASMA-CIGS), Teilprojekt: Entwicklung eines Chalkogenisierungsprozesses auf Basis SEL: Projektlaufzeit 01.11.2011–31.10.2014. Carl von Ossietzky Universität Oldenburg, Institut für Physik, Abt. Energie- und Halbleiterforschung (EHF). 2015;26–27.

22. Herberholz R, Igalson M, Schock HW. Distinction between bulk and interface states in CuInSe$_2$/CdS/ZnO by space charge spectroscopy. J. Appl. Phys. 1998; 83:318.

23. Eisenbarth T, Unold T, Caballero R, Kaufmann CA, Schock H-W. Interpretation of admittance, capacitance-voltage, and current-voltage signatures in Cu(In,Ge)Se$_2$ thin film solar cells. J. Appl. Phys. 2010; 107:034509.

24. Walter T, Herberholz R, Müller C, Schock HW. Determination of defect distributions from admittance measurements and application to Cu(In,Ga)Se$_2$ based heterojunctions. J. Appl. Phys. 1996; 80 (8):4411.

25. Yang K-J, Kim S, Kim S-Y, Ahn K, Son D-H, Kim S-H, et al. Flexible Cu2ZnSn(S,Se)4 solar cells with over 10% efficiency and methods of enlarging the cell area. Nat. Commun. 2019; 10:2959. https://doi.org/10.1038/s41467-019-10890-x PMID: 31273214